Online-Journals.org

iJOE International Journal of Online and Biomedical Engineering

iJOE | eISSN: 2626-8493 | Vol. 22 No. 7 (2026) | OPEN ACCESS

https://doi.org/10.3991/ijoe.v22i07.60077

PAPER

# Integrating Multi-Source Pulmonary X-Ray Data into a Cross-Validated CNN with AdamW and Augmentation

**Fouad Issouani**[1] (✉), **Ayyad Maafiri**[2], **Soumia Ziti**[1,3,4]

[1]Mohammed V University in Rabat, Rabat, Morocco

[2]Cadi Ayyad University, Marrakesh, Morocco

[3]Hassan II University in Casablanca, Casablanca, Morocco

[4]Moroccan Society of Digital Health (SMSD), Rabat, Morocco

fouad.issouani@um5r.ac.ma

**ABSTRACT**

The global spread of COVID-19 has affected health and economic conditions worldwide, and new variants continue to appear despite the availability of vaccines. These variants share a common effect on the respiratory system, which keeps pulmonary disease detection a major priority. This study presents an approach for classifying lung diseases using a tailored convolutional neural network (CNN). The system combines several chest X-ray (CXR) datasets and applies extensive data augmentation to build a balanced dataset and improve generalization. The model distinguishes five classes: Normal, COVID-19, Tuberculosis, Viral Pneumonia, and Bacterial Pneumonia. Cross-validation ensures more stable performance and reduces overfitting risks. The method uses the AdamW optimizer to improve convergence and training stability. Performance evaluation includes confusion matrix indicators such as accuracy, specificity, precision, sensitivity, and F1-score, along with ROC curves. The results show that the method is reliable and efficient for automatic classification of CXR images. The CNN model had an average accuracy of 95.26% and a macro-AUC of 99.32% across five folds. Our model is implemented on the TensorFlow framework with the datasets that are public and available for the research community.

**KEYWORDS**

medical imaging, chest radiography, pulmonary diseases, CNN model, data augmentation, cross-validation

## 1 INTRODUCTION

The COVID-19 (corona virus disease) [1] has corpus-consistently affected people's lives as well as health care systems globally. Health agencies and governments are dealing with a drastic increase in the number of patients requiring hospitalization due to the rapid spread of the virus as well as the serious potential that the disease could have on elderly and chronic health patients were placed under extreme pressure, and health care workers were required to meet the extraordinarily high demand of the virus's spread. Screening tests, such as PCR or serological tests, have been used at the population level, but their availability, cost, and speed

Issouani, F., Maafiri, A., Ziti, S. (2026). Integrating Multi-Source Pulmonary X-Ray Data into a Cross-Validated CNN with AdamW and Augmentation. *International Journal of Online and Biomedical Engineering (iJOE)*, 22(7), pp. 112–125. https://doi.org/10.3991/ijoe.v22i07.60077

Article submitted 2025-12-16. Revision uploaded 2026-03-12. Final acceptance 2026-03-12.

have limitations. Consequently, chest X-ray (CXR) [2]. It has become a fast, least invasive, and widely accessible alternative for diagnostic reasons.

Medical image [3] processing methods have emerged as an automated solution from computer vision methods in recent years [4]. Convolutional neural networks (CNNs) [5] have been demonstrated to be robust to visual feature extraction and the classification of lung [6] diseases in particular. These models, which are composed of a sequence of layers including convolutional layers, pooling layers, and fully connected layers, have already been tested and validated in many areas of medicine [7], including, for instance, the identification of brain tumors, prostate cancer screening, detection [8] of lung abnormalities, and breast lesion analysis. Finally, pixel values are normalized between 0 and 1, which stabilizes network training and accelerates convergence.

This protocol, combining multiple source [9], [10], [11], [12] aggregation, data augmentation, and global preprocessing of all images, ensures optimal consistency and promotes better generalization during the cross-validation phase. The ultimate goal is to provide medical staff with a powerful tool capable of quickly and reliably diagnosing several [13] lung infections [14], including COVID-19, tuberculosis, viral pneumonia, and bacterial pneumonia, in order to support clinical decision-making and improve patient care.

In this study, we used a composite database obtained by merging several public sources of chest images. The results show a significant improvement in the accuracy and sensitivity of the proposed model. The effectiveness of our methodology was also compared to the previous studies to justify its relevance. The remainder of this paper follows the following structure: Section 2 summarizes the recent studies on the lung disease classification [15] by using medical images, and comparing the performance of the current models. Section 3 outlines the suggested methodology, which includes data building, methods of preprocessing and augmentation [16], and the applied CNN [17] structure. Section 4 describes the experimental format, namely the training protocol, hyperparameters adopted, and the measures of evaluation adopted. Section 5 reveals the values of the obtained results, such as precision, recall, F1-score, ROC curves, and confusion matrix scores and a comparison with the previous work. Section 6 gives a conclusion to the article, whereby the working paper summarizes what was contributed by the study and where future directions of works can be done to make the model stronger and easier to interpret.

## 2 RELATED WORKS

Recently, CNN has greatly enhanced its ability to recognize, identify, and classify diseases from not only CXR, but also CT scan images. Its high accuracy in identifying diseases has prompted and encouraged researchers by using deep learning techniques.

Chest imaging-based pulmonary disease diagnostics: Deep learning models have been explored in several recent studies [18], particularly when using small datasets. To categorize the images of COVID-19, viral pneumonia, lung opacities, and normal CXR images, four trained CNNs (VGG16, DenseNet201, Xception, DarkNet19) were evaluated in [14]. While ensemble methods peaked at 97.79% accuracy using 14,777 images, including 2,493 COVID-19 cases, Xception achieved 94.78% accuracy. Perumal et al. Another study [19] used DenseNet201 to achieve 93% accuracy on a small set of 509 images (CT and CXR) by combining transfer learning with Haralick texture features. Another study that evaluated six CNNs to identify COVID-19, pneumonia, and tuberculosis from 5,863 CXR images proposed by [20] in 2025. DenseNet201 and ResNet50 achieved 92% accuracy.

A different 2025 study [21] adapted ResNet-18 to attention modules and was applied to 3,100 images, with the COVID-19, pneumonia, and normal cases being classified with an accuracy of 94.38. In [22] an uncertainty-aware CNN trained on a subset of CXR and tested on 7,800 images, with 95% accuracy of ARDS-related opacities. Lastly [23] trained CNN with 1,840 CXR images (four classes) and obtained 96.74% accurate results. The model has been implemented through a real-life web application.

### 2.1 Recent advancements in Vision Transformers applied to image classification

That said, much of this literature is based on limited datasets, usually examining one or two disease conditions (often just COVID-19 and/or pneumonia). Limitations of these types of datasets contribute to the model's absence and the lack of generalizability to other respiratory diseases [24]. A comparison of current deep learning classification models by dataset size used and the accuracy obtained is presented in Table 1.

**Table 1.** Performance comparison of current deep learning classification models by dataset size and accuracy

| Study | Diseases | Models | Dataset Size | Medical Imaging | Accuracy (%) |
|---|---|---|---|---|---|
| [14] | COVID-19, Viral Pneumonia, Lung Opacity, Normal | VGG16, DenseNet201, DarkNet19, Xception, Ensemble | 14,777 | Chest X-Ray (CXR) | 94.78 |
| [19] | COVID-19 | DenseNet201 + Haralick Features | 5,232 | CT & CXR | 93 |
| [20] | COVID-19, Pneumonia, Tuberculosis | ResNet50, DenseNet201, VGG16, InceptionV3, MobileNet, Xception | 5,863 | Chest X-Ray (CXR) | 92 |
| [21] | COVID-19, Pneumonia, Normal | ResNet-18+ Attention | 3,100 | Chest X-ray | 94.38 |
| [22] | Bilateral Opacities | Uncertainty-Aware CNN | 7,800 | Chest X-ray | 95 |
| [23] | Normal, Pneumonia, COVID-19, TB | CNN (custom) | 1,840 | Chest X-ray | 96.74 |

In contrast, our work is distinct because our model relies on a composite [25] and enriched dataset consisting of various CXR images for multiple pathologies: COVID-19, tuberculosis, viral pneumonia, bacterial pneumonia, and normal.

We managed to select a sufficiently large and well-balanced image corpus by means of the combination of various publicly accessible data and the usage of systematic data augmentation protocols, which enabled us to train a model with high robustness, stability, and generalizability.

## 3 METHODOLOGY

### 3.1 Dataset description

We assembled a composite dataset of the chest X-rays to train the model by drawing on a number of publicly available databases of X-rays:

The COVID-19 Image Repository [9], created by Hannover Medical School (MHH) via the Institute for Diagnostic and Interventional Radiology.

The COVID-19 Image Data Collection [10], It is one of the first publically available datasets that were published during the beginning of the pandemic.The BIMCV-COVID19+ [11], [12], one of the largest public databases of medical images related to COVID-19.

The initial set contained 28,627 chest X-rays, divided into five diagnostic categories:

- 11,109 normal cases.
- 4,192 COVID-19 positive cases.
- 5,699 tuberculosis cases.
- 5,618 viral pneumonia cases.
- 2,009 bacterial pneumonia cases.

## 3.2 Preprocessing

This set presented an imbalance between classes, with less data available for bacterial pneumonia and COVID-19. We applied data augmentation to overcome this limitation, this method wherein the images are manipulated. This included rotating, zooming, flipping both horizontally and vertically, and making small scaling adjustments. This step saw us through successfully balancing the classes so that we could artificially generate new images and train the model to generalize as a whole. By doing this, the final dataset was boosted to 49,332 X-ray images, which were now evenly balanced across the five categories. The balance provided a better foundation on which to construct a high-quality and stable model. The sets of images in the database are distributed:

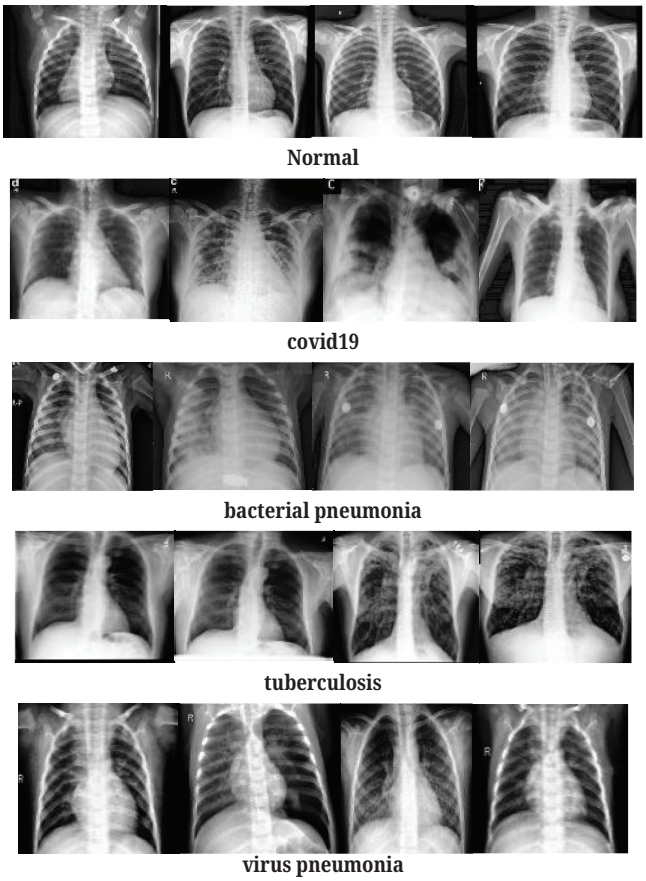


**Fig. 1.** Some images from the dataset used

All the images in Figure 1 went through an orderly process of sanitizing their format (grayscale), being scaled down to 224 × 224 pixels, & normalizing the pixel intensity to be between zero and one prior to inclusion into the network. The goal of these processes is to provide a level of uniformity across diverse imaging classes, as well as automate the classification of chest x-rays for lung disease using a CNN that will discover a model capable of identifying patients with lung disease in multiple diagnostic categories including: SARS-CoV-2 (COVID-19), tuberculosis, and viral, bacterial and normal pneumonia.

- Image preprocessing and classification: Each image from the set of chest x-rays was categorized by one of five classes. Once assigned, the images were converted to grayscale format (for a simpler visual appearance but maintain the essential structural data to provide diagnostic information) prior to their inclusion into the deep learning model.
- Population of image data: All x-ray images were resized to a pixel resolution of 224 × 224 pixels (i.e. our CNN was designed to accept 224 × 224 pixels input data). All image pixel data were converted from integers to floating point, normalized to a range of 0–1, per: 0 to 1
  Image Intensity + 1 Image Intensity (1):

$$I_{\text{norm}}(x, y) = \frac{I(x, y)}{255}$$

  $I(x, y)$: represents the intensity of a pixel in the original image.
  $I_{\text{norm}}(x, y)$: represents the normalized intensity.

This process allows for stabilization of training and improves convergence of the neural network.

Balancing the dataset via augmentation. The first dataset had an uneven distribution across classes, especially for bacterial pneumonia and COVID-19. To resolve this, we employed geometric transformations that indicate the artificial generation of new images. using the following equations

Rotation by an angle θ:
Translation of a vector $(t_x, t_y)$: $(x', y') = (x + t_x, y + t_y)$
Zoom or Scale with a factor $s$: $(x', y') = (s \cdot x,\ s \cdot y)$

These transformations, combined with horizontal/vertical flips and brightness modifications, increased the size of the dataset to a total of 49,332 X-rays balanced across the five classes.

## 3.3 Balancing the dataset via augmentation

The first data set showed an extremely imbalanced data set between classes of pulmonary diseases, the large portion of the data set was made up of either bacterial pneumonia or COVID. To help adjust for this issue so that the learning process had an equitable development experience of learning, various data augmentation techniques were used within the training set to allow for adjustments to be made during the learning process. The data augmentations used on the training set included rotation of images, flipping both horizontally and vertically, adding different scales of size, and adding different zooms to the images.

The purpose of using these various augmentation transformations was to eventually create a greater level of diversity in the training samples while maintaining the actual medical characteristics of the CXR images. As a result of these processes, the actual volume of the data set has increased from 28,627 original images to 49,332 augmented images with a more uniform distribution of the five diagnostic results throughout the four original classes than existed initially. This balancing strategy helps the CNN model learn more representative patterns and reduces the risk of bias toward majority classes during training.

### 3.4 Cross-validation strategy and data leakage prevention

In order to have an unbiased view of the proposed model's performance, a stratified five-fold cross-validation approach occurred during training. There were five folds, made with respect to maintaining as close to the same distribution of classes across each subset. Four of the folds were used as training data and the remaining fold was used as validation data. Each fold was used as the validation fold for one of the five iterations. To minimize the possibility of data leakage, all augmentation methods were applied to the training folds only during each iteration of the cross-validation process. Only the original images were present in the validation fold, and no data augmentation was being done. Therefore, the validation performance will give an accurate measure of the ability to generalize outside of the training/validation dataset as testing on augmented data may inflate the validation performance, as an example. The dataset was made up from multiple publicly available databases, and therefore, complete patient-level identifiers were not always available for each subject. Therefore, while a strict separation by patient was not possible, careful procedures for data partitioning and cross-validation were used to limit potential bias and provide a thorough evaluation of the model across all five classes of pulmonary diseases.

### 3.5 Convolution neutral network architecture

In this research, we used a CNN architecture designed to classify multiple types of lung diseases based on CXR images. While the design is similar to other CNN, it has a customized configuration of convolutional, pooling, dropout, and fully connected layers that correspond to the characteristics of grayscale CXR images. Input to the network is a 224 by 224 pixels grayscale image. The increasing number of filters provides the ability to capture both low, medium, and high levels of radiographic patterns for use in identifying pulmonary disease.

The model consists of several convolutional blocks (32, 64, 128 filters) followed by pooling and regularization (dropout) layers. The extracted [26] features are then flattened and passed to a fully connected layer (256 neurons, ReLU activation), then to a Softmax output layer with 5 neurons corresponding to the diagnostic classes. The images were then split into two sets: the training/validation set, which was the set used in cross-validation, and the test set, which was held out for the final evaluation of the model.

A CNN architecture [27] was then designed to build our classification model.

This architecture is defined as follows:

- Three convolutional blocks [28], successively applying filters of 32, 64, and 128 with kernels of size 3×3, each followed by a ReLU activation function.

- Each block is followed by a MaxPooling layer (2 × 2) to reduce the feature map dimensions by half.
- To eliminate overfitting, dropout layers are added (25 percent in the first 2 blocks and 30 percent in the final block).
- A Flatten layer to convert the feature maps into a one-dimensional vector.
- 1st 256-neuron dense layer with ReLU activation, then 2nd 30-percent Dropout.
- The final dense layer comprises five neurons and a Softmax activation function, which classifies the following five categories: Normal, COVID-19, Tuberculosis, Viral Pneumonia, and Bacterial Pneumonia.
- Breakdown of data into learning and validation sets:

A stratified five-fold cross-validation method evaluated the training data. In each iteration, four folds were used for training and one fold was used for validation.

Figure 2 illustrates the CNN architecture employed in this study:

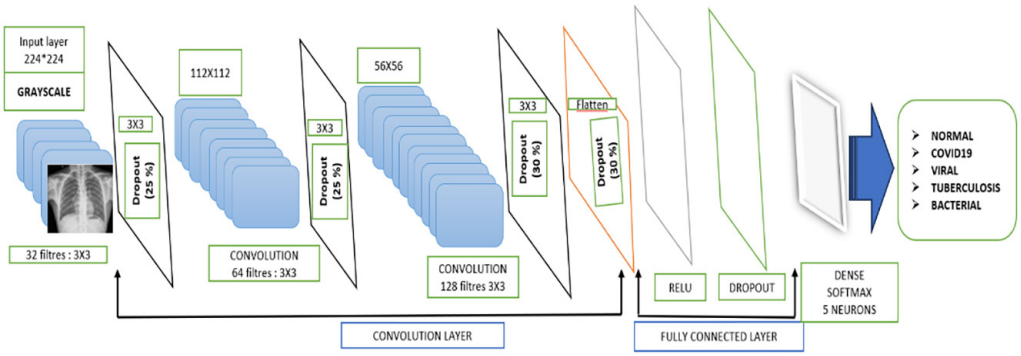


**Fig. 2.** The architecture of the CNN used

The CNN [23] structure was built by selecting the number and types of convolutional and fully connected layers.

For training, we employed the AdamW optimizer [29] with categorical cross-entropy loss. The training was performed with a batch size of 32 with a maximum of 20 epochs and using strategies for early stopping and a reduced learning rate in order to stabilize convergence.

When the training was complete, the model was assessed for performance using accuracy, specificity, precision, sensitivity, F1 score, and the receiver operating characteristic (ROC) curve. The confusion matrix was also created to review the distribution of true positives (TP), true negatives (TN), false positives (FP), and false negatives (FN). These indicators provide a detailed assessment of the classification performance across all five disease categories.

## 3.6 Ethical considerations (Human data statement)

Ethical approval and use of human data. This research did not involve any direct experimentation on human subjects. The databases used (e.g., CIR [9], CIDC [10], BIMCV+ [11], [12]) are public, fully anonymized, and comply with applicable ethical and legal standards. In accordance with institutional and international guidelines, no additional ethical approval was required for this secondary analysis of anonymized data. No identifiable personal, clinical, or biometric information was collected, processed, or disseminated.

## 4 RESULTS

As can be seen from Table 1 above, the CNN model's class-level performance is also analyzed. Each row is a pulmonary category, and the mean precision, recall, and F1-score were computed following cross-validation.

The NORMAL class is performing great, reaching 96% for both precision and recall, which shows how the model is very stable.

The most difficult class to distinguish is COVID-19, resembling tuberculosis or viral pneumonia in the visuals of X-rays.

TUBERCULOSIS gives a competitive performance with a slight lack of stability on certain training folds.

The results concerning Viral Pneumonia are very consistent, demonstrating the robustness of our model for this type of pathology.

Bacterial Pneumonia class achieves almost perfect performance (≈100%), which demonstrates excellent detection capability and very low confusion with other classes.

**Table 2.** Comparative overview of related studies based on dataset size and Accuracy

| Class | Average Precision | Average Recall | Average F1-Score |
|---|---|---|---|
| NORMAL | ≈ 96%–98% | ≈ 95%–98% | ≈ 96%–97% |
| COVID-19 | ≈ 78%–90% | ≈ 88%–93% | ≈ 85%–90% |
| TUBERCULOSIS | ≈ 89%–94% | ≈ 78%–93% | ≈ 85%–91% |
| Viral PNEUMONIA | ≈ 94%–98% | ≈ 94%–97% | ≈ 96%–97% |
| Bacterial PNEUMONIA | ≈ 99%–100% | ≈ 99%–100% | ≈ 99%–100% |

These observations in Table 2 confirm the reliability of the model proposed, and at the same time highlight areas of potential confusion between certain lung conditions, particularly between COVID-19 and other forms of pneumonia.

**Table 3.** Evaluation results

| Study | Dataset Size | Accuracy (%) |
|---|---|---|
| [14] | 14,777 | 94.78 |
| [19] | 5,232 | 93 |
| [20] | 5,863 | 92 |
| [21] | 3,100 | 94.38 |
| [22] | 7,800 | 95 |
| [23] | 1,840 | 96.74 |
| **Proposed method** | **49,332** | **95.26 (±1.35)** |

In Table 3, we assessed our approach on a rich and balanced dataset of chest X-rays across multiple lung diseases for our evaluation. The experimental evaluation tested the effect of image preprocessing steps and data augmentation on overall classification performance. Our results were benchmarked against other available CNN-based architectures, including ResNet and DenseNet variants. The results showed

consistent improvements across most metrics, a summary of which can be seen in the table, along with precision per class.

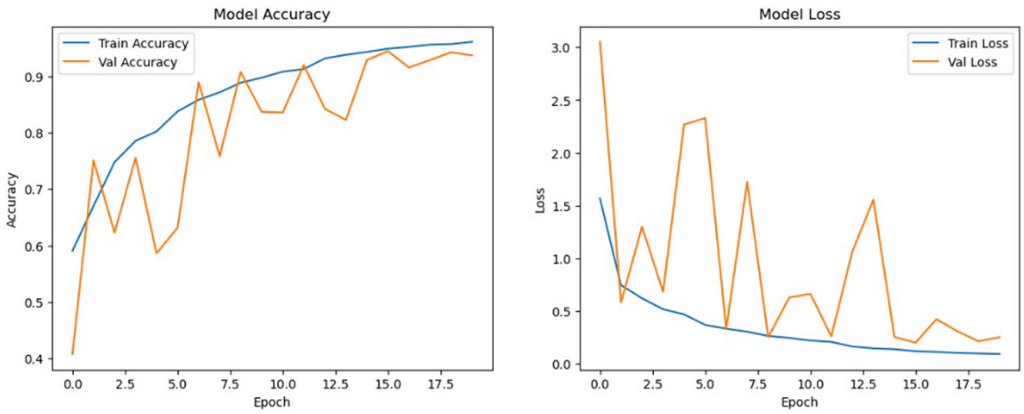


**Fig. 3.** Training and validation performance curves of the proposed CNN

Figure 3 illustrates the behavior of training accuracy (blue) steadily grows and flattens at 95.5%, whereas the validation accuracy (orange) grows in the same direction with certain fluctuations caused by data augmentation, and the loss in training gradually drops, and the loss in validation is minimal, which proves the existence of good convergence and generalization. These curves indicate that the suggested CNN utilizes the big multiclass dataset to learn without overfitting.

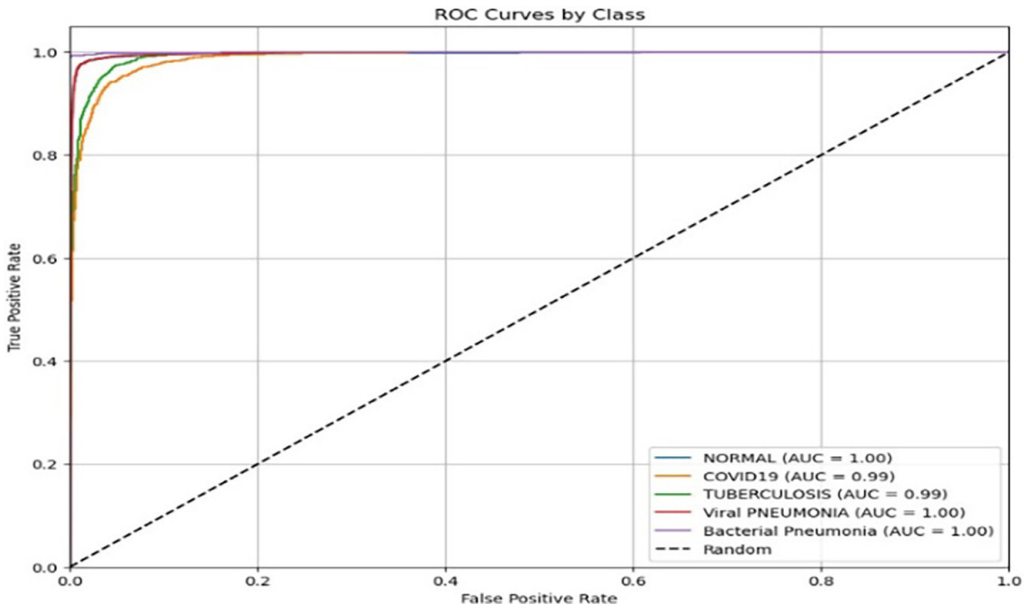


**Fig. 4.** ROC curves of the proposed CNN model for each pulmonary class

The curves in Figure 4 show high levels of class separation with the values of the AUC between 0.99 and 1.00. The model attained a macro-AUC of 0.9932, which indicates its adequacy in discriminating the presence of similar lung diseases like COVID-19, viral pneumonia, and tuberculosis. The curves are all well above the random diagonal, which means that the classifier is highly discriminative and stable.

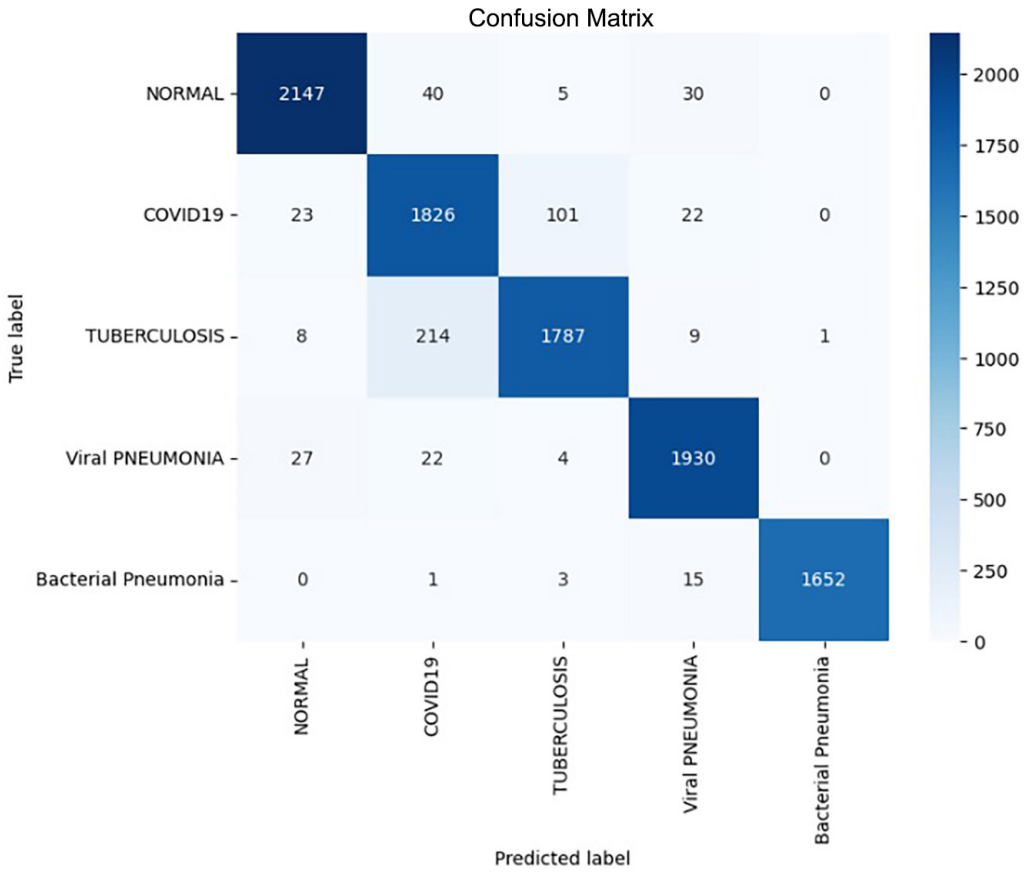


**Fig. 5.** Confusion matrix of the proposed CNN model

The diagonal dominance in Figure 5 confirms high classification accuracy across all five pulmonary classes. The most frequent misclassification occurs between COVID-19 and Tuberculosis, due to their similar radiographic patterns. The Bacterial Pneumonia and Viral Pneumonia classes show near-perfect detection, with overall robustness supported by a large and balanced dataset (≈ 49k images).

## 5 DISCUSSION

The results demonstrate that our model achieves good classification performance for the five diagnosed pulmonary diseases. The model achieved an accuracy rate of approximately 99–100% for the bacterial pneumonia, viral pneumonia and Normal classes, and performed comparably to – or even higher than – previous studies which typically reported an average accuracy percentage between 92–97%. The proposed study is also a more challenging multi-class classification problem than previous research has attempted. For example, Al-Issa et al. (2022) achieved 94% accuracy using Xception on a four-class classification problem. In contrast, the authors of this study have indicated five diagnosis classes making this a much more complex classification problem; however, there were no significant drops in performance on the five classifications classes compared to Al-Issa et al. (2022). The COVID-19 classification produced an accuracy of approximately 78–90% and recall of between 88–93% which are lower than many past literature examples (93–96%); however, this may be due to the additional classifications involved with multi-class classification and the number of new classifications may have introduced additional variance within

the data. Another important aspect of this work is the use of a relatively large and heterogeneous dataset compared with many previous studies that focused on fewer disease categories and smaller datasets (often fewer than 6,000 images). In addition, the application of data augmentation techniques helped improve the robustness of the learning process and reduce the effects of class imbalance.

It is also worth noting that the classification performance obtained for the bacterial pneumonia class is particularly high compared with the other disease categories. While this result demonstrates the ability of the CNN model to identify discriminative radiographic patterns, it may also partially reflect characteristics of the datasets used in this study. Since the images were collected from multiple public repositories, differences in image acquisition protocols, annotation procedures, or class-specific visual patterns may introduce subtle dataset biases that make certain classes easier to classify. Future work should therefore include evaluation on independent external datasets and clinical data collected in hospital environments in order to better assess the generalization capability of the proposed model. Overall, the results indicate that the proposed CNN-based framework provides competitive performance for multi-class pulmonary disease classification while maintaining a comprehensive evaluation using multiple metrics such as precision, recall, F1-score, confusion matrices, and ROC curves.

## 6 CONCLUSION

In our work, we put forward a CNN-based model that was able to classify five pulmonary conditions, namely normal, COVID-19, tuberculosis, viral pneumonia, and bacterial pneumonia, based on the images of the chest X-rays. The model was highly performing with particularly good results on bacterial and viral pneumonia, where the precision, recall, and F1-scores were always above 96%. The model was also robust and generalizable even in more demanding classes such as COVID-19 and tuberculosis. Our approach is superior to the existing literature in terms of its inclusion of a composite and balanced dataset, systematic data augmentation, and a multi-metric assessment plan, in comparison with the literature that, in most cases, depended on smaller datasets and fewer disease categories. This enabled a more reliable and clinically relevant classification system.

**Future Work.** Combine interpretable AI methods (eg, Grad-CAM) for facilitating clinical interpretability. Combine the dataset with more rare cases to improve coverage. Consider real-time screening using slim architectures or mobile deployment. Validate your model by external datasets and collaboration with hospitals. Evaluates scalability against newer architectures such as Vision Transformers."

## 7 REFERENCES

[1] H. Benradi, A. Chater, and A. Lasfar, "Detection of COVID-19 from chest radiology using histogram equalization combined with a CNN convolutional network," *ITM Web Conf.*, vol. 46, p. 05001, 2022. https://doi.org/10.1051/itmconf/20224605001

[2] H. Benradi, I. Bouganssa, A. Chater, and A. Lasfar, "Discriminative approach lung diseases and COVID-19 from chest X-ray images using convolutional neural networks: A promising approach for accurate diagnosis," *Int. J. Online Biomed. Eng. IJOE*, vol. 19, no. 14, pp. 131–141, 2023. https://doi.org/10.3991/ijoe.v19i14.42725

[3] F. Issouani, A. Maafiri, and S. Ziti, "Advances in medical image segmentation: A comparative study of hybrid CNN-transformer architectures and specialized AI models," in *Progress in Intelligent Computing and Secure Communication Systems*, in Lecture Notes in Networks and Systems, C. El Mokhi, H. Hachimi, N. Hmina, and A. Addaim, Eds., vol. 1555, Springer, Charm, 2025, pp. 90–98. https://doi.org/10.1007/978-3-031-99997-0_9

[4] M. Y. Achibat, N. Aqili, and S. Ziti, "Bibliometric analysis of advances in artificial intelligence in healthcare and medicine," in *HealthTech "Global Summit of Digital Health*, in Lecture Notes in Networks and Systems, W. Rhalem, N. Al Idrissi, and M. Lazaar, Eds., vol. 1587, Springer, Charm, 2026, pp. 321–329. https://doi.org/10.1007/978-3-032-01970-7_31

[5] L. Moraes Armesto, T. Roberto Alonso, D. Souza Ferreira Magalhães, and L. Dos Santos, "Artificial neural networks as a support and learning tool in medical practice," *Int. J. Online Biomed. Eng. IJOE*, vol. 21, no. 13, pp. 151–168, 2025. https://doi.org/10.3991/ijoe.v21i13.58335

[6] B. H. Prasetio and M. A. Z. Anam, "Portable real-time edge-based AI system for respiratory disease diagnosis via breath sound analysis with adaptive gated fusion of acoustic features," *Int. J. Online Biomed. Eng. IJOE*, vol. 21, no. 13, pp. 31–45, 2025. https://doi.org/10.3991/ijoe.v21i13.56689

[7] W. Abbaoui, S. Retal, N. Kharmoum, and S. Ziti, "Artificial intelligence at the service of precision medicine," in *International Conference on Advanced Intelligent Systems for Sustainable Development*, in Lecture Notes in Networks and Systems, J. Kacprzyk, M. Ezziyyani, and V. E. Balas, Eds., vol. 713, Springer, Charm, 2023, pp. 91–103. https://doi.org/10.1007/978-3-031-35248-5_9

[8] T. T. Mac, X. T. Nguyen, H. A. Bui, T. H. Nguyen, and H. H. Ly, "An attention-enhanced hybrid deep learning model based on VGG16 and VGG19 for pneumonia detection from chest X-ray images," *Int. J. Online Biomed. Eng. IJOE*, vol. 21, no. 12, pp. 63–83, 2025. https://doi.org/10.3991/ijoe.v21i12.55953

[9] H. B. Winther *et al.*, "COVID-19 image repository," *LUIS*, 2020. https://doi.org/10.25835/0090041

[10] J. P. Cohen, P. Morrison, and L. Dao, "COVID-19 image data collection," *arXiv preprint arXiv:2003.11597*, 2020. https://doi.org/10.48550/ARXIV.2003.11597

[11] M. de la Iglesia Vayá *et al.*, "BIMCV COVID-19+: A large annotated dataset of RX and CT images from COVID-19 patients," *IEEE DataPort*, 2021. https://doi.org/10.21227/W3AW-RV39

[12] M. de la I. V. de la Iglesia Vayá and J. M. S.-T. Saborit-Torres, "BIMCV COVID-19+: A large annotated dataset of RX and CT images from COVID-19 patients with Extension Part I," *IEEE DataPort*, 2026. https://doi.org/10.21227/F3Q6-0986

[13] T. T. Mac, X. T. Nguyen, H. A. Bui, T. H. Nguyen, and H. H. Ly, "An attention-enhanced hybrid deep learning model based on VGG16 and VGG19 for pneumonia detection from chest X-ray images," *Int. J. Online Biomed. Eng. IJOE*, vol. 21, no. 12, pp. 63–83, 2025. https://doi.org/10.3991/ijoe.v21i12.55953

[14] Y. Al-Issa, A. Mohammad Alqudah, H. Alquran, and A. Al Issa, "Pulmonary diseases decision support system using deep learning approach," *Comput. Mater. Contin.*, vol. 73, no. 1, pp. 311–326, 2022. https://doi.org/10.32604/cmc.2022.025750

[15] H. Sabbar, H. Silkan, and K. Abbad, "Deep learning-based real-time classification of thoracic pathologies in chest radiographs," *Int. J. Online Biomed. Eng. IJOE*, vol. 21, no. 14, pp. 20–37, 2025. https://doi.org/10.3991/ijoe.v21i14.58193

[16] R. Zeng *et al.*, "Power quality data augmentation and processing method for distribution terminals considering high-frequency sampling," *Energies*, vol. 18, no. 24, p. 6426, 2025. https://doi.org/10.3390/en18246426

[17] F. Issouani, A. Maafiri, and S. Ziti, "Robust deep learning model for lung disease diagnosis," in *HealthTech "Global Summit of Digital Health"*, in Lecture Notes in Networks and Systems, W. Rhalem, N. Al Idrissi, and M. Lazaar, Eds., vol. 1586, Springer, Charm, 2026, pp. 40–48. https://doi.org/10.1007/978-3-032-01967-7_5

[18] M. Sanjay, R. S. Kanaparthi, M. Pillaram, and J. Balaji, "AI for rare disease diagnosis via skin and eye images," *J. Future Soc. Educ.*, vol. 2, no. 4, pp. 4–19, 2025. https://doi.org/10.3991/jfse.v2i4.56537

[19] V. Perumal, V. Narayanan, and S. J. S. Rajasekar, "Detection of COVID-19 using CXR and CT images using Transfer Learning and Haralick features," *Appl. Intell.*, vol. 51, no. 1, pp. 341–358, 2021. https://doi.org/10.1007/s10489-020-01831-z

[20] M. H. Al-Adhaileh *et al.*, "DLAAD-deep learning algorithms assisted diagnosis of chest disease using radiographic medical images," *Front. Med.*, vol. 11, p. 1511389, 2025. https://doi.org/10.3389/fmed.2024.1511389

[21] K. Ahmad, H. U. Rehman, B. Shah, F. Ali, and I. Hussain, "Dual-model approach for accurate chest disease detection using GViT and swin transformer V2," *Sci. Rep.*, vol. 15, no. 1, p. 31717, 2025. https://doi.org/10.1038/s41598-025-16422-6

[22] M. Arora *et al.*, "Uncertainty-aware convolutional neural network for identifying bilateral opacities on chest X-rays: A tool to aid diagnosis of acute respiratory distress syndrome," *Bioengineering*, vol. 10, no. 8, p. 946, 2023. https://doi.org/10.3390/bioengineering10080946

[23] N. O. Adiwijaya, B. S. Miranda, and D. I. Swasono, "CNN-based classification of infectious lung diseases using thorax X-ray analysis," *Eng. Technol. J.*, vol. 9, no. 10, pp. 5348–5353, 2024. https://doi.org/10.47191/etj/v9i10.14

[24] B. H. Prasetio and M. A. Z. Anam, "Portable real-time edge-based AI system for respiratory disease diagnosis via breath sound analysis with adaptive gated fusion of acoustic features," *Int. J. Online Biomed. Eng. IJOE*, vol. 21, no. 13, pp. 31–45, 2025. https://doi.org/10.3991/ijoe.v21i13.56689

[25] A. Maafiri, K. Chougdali, A. Bir-Jmel, and N. Ababou, "Improved fusion of SVD and relevance weighted LDA algorithms via symmetric sum-based rules for face recognition," in *Digital Technologies and Applications*, in Lecture Notes in Networks and Systems, S. Motahhir and B. Bossoufi, Eds., vol. 669, Springer, Charm, 2023, pp. 472–481. https://doi.org/10.1007/978-3-031-29860-8_48

[26] A. Maafiri, Y. Himeur, K. Chougdali, S. Atalla, W. Mansoor, and S. Ziti, "SAE-EDA: Sparse autoencoder-based feature extraction and exponential discriminant analysis for robust face recognition," in *Social Robotics*, in Lecture Notes in Computer Science, O. Palinko, L. Bodenhagen, J.-J. Cabibihan, K. Fischer, S. Šabanović, K. Winkle, L. Behera, S. S. Ge, D. Chrysostomou, W. Jiang, and H. He, Eds., vol. 15563, Springer, Charm, 2025, pp. 39–53. https://doi.org/10.1007/978-981-96-3525-2_4

[27] A. Chater, A. Lasfar, and H. Benradi, "A combined method based on CNN architecture for variation-resistant facial recognition," *Int. J. Electr. Comput. Eng. Syst.*, vol. 14, no. 9, pp. 993–1001, 2023. https://doi.org/10.32985/ijeces.14.9.4

[28] A. Maafiri, O. Elharrouss, S. Rfifi, S. A. Al-Maadeed, and K. Chougdali, "DeepWTPCA-L1: A new deep face recognition model based on WTPCA-L1 norm features," *IEEE Access*, vol. 9, pp. 65091–65100, 2021. https://doi.org/10.1109/ACCESS.2021.3076359

[29] H. Arshad, T. Abdullah, M. Rehman, A. Hussain, F. Kanwal, and M. Parveen, "Optimizer-aware fine-tuning of whisper small with low-rank adaption: An empirical study of Adam and AdamW," *Information*, vol. 16, no. 11, p. 928, 2025. https://doi.org/10.3390/info16110928

## 8 AUTHORS

**Fouad Issouani** is a researcher at the IPSS Laboratory (Intelligent Processing and Security of Systems) at Faculty of Science, Mohammed V University in Rabat. His research focuses on deep learning for medical image classification, particularly multiclass CNN models, radiographic image analysis, and data augmentation for improved generalization in healthcare applications (E-mail: fouad.issouani@um5r.ac.ma).

**Ayyad Maafiri** received the Ph.D. degree in computer science from Ibn Tofail University, Kenitra, Morocco, in 2023. He is currently an Assistant Professor with the Multidisciplinary Faculty of Safi, Cadi Ayyad University, Morocco. His research interests include machine learning, biometrics, computer vision, image analysis, and pattern recognition, with an emphasis on developing innovative AI-driven solutions for real-world applications (E-mail: a.maafiri@uca.ac.ma).

**Dr. Soumia Ziti** is a Full Professor and researcher at the Intelligent Processing and Security of Systems, Faculty of Science, Mohammed V University in Rabat since 2007. She obtained her PhD in computer science specializing in graph theory from the University of Orleans in France, along with a diploma in advanced studies in fundamental computer science. She also holds a Baccalaureate in Mathematical Sciences and completed her undergraduate studies in mathematics and physics, specializing in mathematics, at Hassan II University in Morocco. Furthermore, she earned a master's degree in science and technology in computer science from the same institution. Her research interests encompass a wide range of topics including graph theory, information systems, artificial intelligence, data science, software development, database modelling, big data, cryptography, and numerical methods and simulations. Pr. Ziti has contributed extensively to these fields with over than eighty publications in esteemed international journals and conferences. Additionally, she plays a pivotal role in coordinating, participating or assessing in various educational and socio-economic or research projects (E-mail: s.ziti@um5r.ac.ma).